Resonances in finite-size all-dielectric metasurfaces for light trapping and propagation control

Nikita Ustimenko,[1,*] Carsten Rockstuhl,[1,2] and Andrey B. Evlyukhin[3,†]

[1]*Institute of Theoretical Solid State Physics, Karlsruhe Institute of Technology, Kaiserstr. 12, 76131 Karlsruhe, Germany*

[2]*Institute of Nanotechnology, Karlsruhe Institute of Technology, Kaiserstr. 12, 76131 Karlsruhe, Germany*

[3]*Institute of Quantum Optics, Leibniz University Hannover, Welfengarten 1, 30167 Hannover, Germany*

(Received 20 November 2023; revised 26 February 2024; accepted 29 February 2024; published 28 March 2024)

We investigate the development and tuning of resonant optical effects in finite-size periodic arrays (metasurfaces) of silicon nanoparticles. By applying Green's tensor formalism and the coupled dipole approximation while incorporating electric and magnetic dipole moments, we outline a theoretical framework to model the optical response of such nanoparticle arrays. We consider the resonant optical response of finite-size arrays as a function of the nanoparticle (unit cell) number in two distinct scenarios of collective resonances: the lattice resonant Kerker effect, which is a complete suppression of the backward scattering, and the quasi-bound state in the continuum. Our developed models and findings provide a pathway for extracting crucial details about the lattice period and the required array size for the experimental observation of collective resonances. These resonances are typically predicted under the assumption of an infinite periodic lattice. By bridging the theoretical predictions with practical considerations, our results contribute to better understanding of specific conditions needed to experimentally observe these collective resonances in finite-size arrays.

DOI: 10.1103/PhysRevB.109.115436

I. INTRODUCTION

All-dielectric nanophotonics exploits subwavelength particles (nanoparticles) as building blocks (meta-atoms) of nanophotonic planar optical devices [1]. These nanoparticles are usually made from a dielectric or semiconductor material with a high refractive index ($n \sim 3$–4). Single nanoparticles and complex planar arrangements provide extremely efficient control of light at the nanoscale through an electromagnetic response inaccessible to bulk materials. This response occurs due to resonances sustained in these high-index dielectric nanoparticles at visible and near-infrared wavelengths [2–5] and associated with the excitation of multipoles [6–9] (see, e.g., Fig. 1).

It was important to appreciate that dielectric, nonmagnetic nanoparticles support not only electric multipoles but also magnetic multipoles [4,5]. Interference of electric and magnetic multipoles can be used to control the directivity and amplitude of the scattered light. For example, at a specific wavelength, the incident linear-polarized plane wave can induce in an isotropic spherical nanoparticle orthogonal magnetic dipole (MD) and electric dipole (ED) moments of equal strength that are oscillating in phase (first Kerker condition [10]). The interference between scattered fields generated by such ED and MD leads to the suppression of scattering in the backward direction relative to the incident light, and it is known as the Kerker effect [2,11–13]. In the case of a single spherical nanoparticle, ED and MD resonances do not overlap, making the Kerker effect a nonresonant phenomenon. However, we note that, by changing the particle shape, an overlap of these resonances in individual particles can be obtained [14] and a resonant Kerker effect emerges for a certain illumination direction [15].

Two-dimensional (2D) periodic arrangements of nanoparticles placed at the lattice nodes, metasurfaces, bring extra degrees of freedom to control spectral positions of multipole resonances [2,16–24]. That is possible because the interaction of the particles within the lattice renormalizes their optical properties. Similar to the cases of 2D arrays of *metallic* nanoparticles supporting so-called plasmonic surface lattice resonances (SLRs) [25–35], the electromagnetic response of a dielectric nanoparticle structure can also be determined by collective modes, known as *collective* or *lattice resonances*, formed by electromagnetic coupling between multipoles of nanoparticles [36]. In this regard, the particle configuration strongly affects the nature and strength of the multipole coupling between particles. For example, it is possible to achieve a spectral overlap of ED and MD collective resonances for a rectangular lattice of spherical nanoparticles at a specific wavelength by independently varying the lattice periods in different directions. As a consequence, the *resonant lattice Kerker effect* emerges, leading to the resonant suppression of backward scattering and reflection from a subdiffraction lattice [37]. The resonant behavior of the lattice Kerker effect can be useful in light sources [29], narrow-band photodetectors [38], and sensing [39].

Another fascinating collective phenomenon exhibited by nanoparticle structures is the accumulation (or trapping) of light energy in the near field of the structures. In the ideal scenario of an infinite lattice, this effect arises due to the presence of *trapped modes* that are also called *bound states in the continuum*. For these resonances, the resonant

*nikita.ustimenko@kit.edu

†evlyukhin@iqo.uni-hannover.de

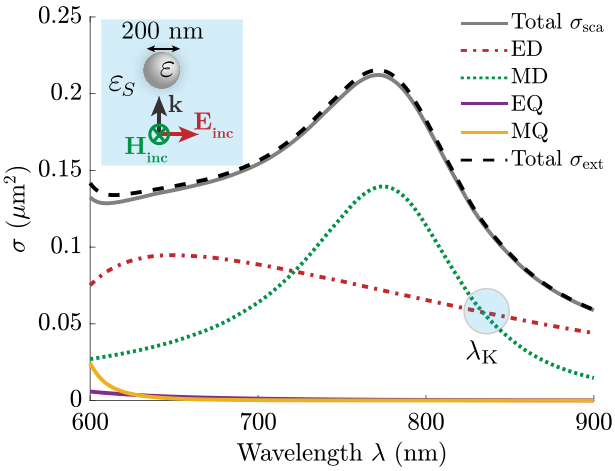

FIG. 1. Extinction cross section σ_{ext} (ECS), scattering cross section σ_{sca} (SCS), and contributions to the SCS from electric dipole (ED), magnetic dipole (MD), electric quadrupole (EQ), and magnetic quadrupole (MQ) for a silicon nanoparticle illuminated by a plane wave propagating in the medium with $n_S = \sqrt{\varepsilon_S} = 1.4$ (see the inset). The blue circle indicates the wavelength $\lambda_K = 834$ nm at which the first Kerker condition is satisfied. The values of the wavelength λ are indicated for vacuum.

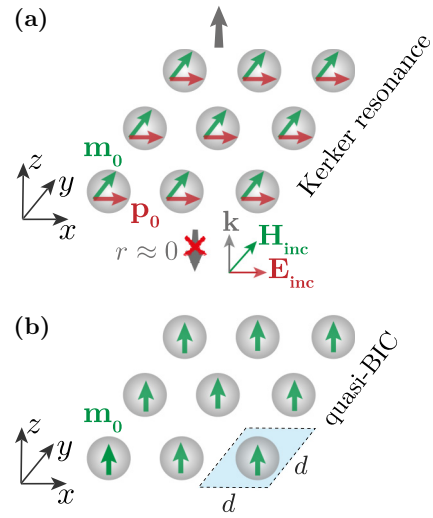

FIG. 2. Illustration of the considered collective resonant effects in a periodic finite-size metasurface of subwavelength-separated Si particles ($d < \lambda/n_S$) with a square unit cell. (a) Lattice Kerker resonance: at the Kerker wavelength, a normally incident plane wave can resonantly induce electric and magnetic dipoles with the same amplitude in each particle due to the overlapping of collective ED and MD resonances. The scattered field from these dipole moments yields zero reflection from the metasurface. (b) Nonradiant trapped eigenmode: dipole bound state in the continuum. For the magnetic dipole BIC, all particles have the same MD moment with the out-of-plane orientation $\mathbf{m}_0 \parallel \mathbf{e}_z$.

frequency is embedded into the continuum of propagating waves in the surrounding medium but without radiation into this medium [19,40–43]. In finite-size structures, the ideal bound states in the continuum are always converted to quasi-bound states in the continuum (quasi-BICs). The observable radiative quality factor (Q factor) is finite but large. The details depend on the array size, as shown for a one-dimensional (1D) chain of particles [44]. From a practical perspective, quasi-BICs are even more useful than the bound states in the continuum, being only ideal mathematical objects, since the quasi-BICs can be excited by an external field. Much like the BICs, the energy of quasi-BICs remains concentrated predominantly within or in close proximity to a dielectric structure. This confinement leads to a considerable enhancement of the light at the nanoscale. That allows us to exploit quasi-BICs in dielectric metasurfaces to enhance nonlinear effects [45], for lasing [46], biosensing [47,48], and multiplexing [49].

Thus, collective resonances in 2D periodic structures have demonstrated great opportunities to control light propagation and concentration at the nanoscale. Even though these periodic arrays are finite in reality, they are frequently represented as infinitely large and perfectly periodic during theoretical modeling. However, the response of finite-size arrays depends on the number of particles and can be significantly different compared to that of an infinite array, even for a sufficiently large number of particles [22,28,29,31,34,35,44,50–56]. It is crucial to investigate the influence of the array size on the resonant effects. Moreover, in experiments on the optical collective effect in metasurfaces, one always deals with finite-dimensional structures of nanoparticles, while numerical simulations usually refer to infinite periodic structures. In this regard, difficult questions arise as to what extent numerical simulations can predict the properties of systems with finite sizes and how numerical simulations can be related to actual experimental implementations.

In this paper, we investigate the emergence and development of collective resonant effects arising from the dipole coupling in finite-size arrays of *dielectric* Mie-resonant nanoparticles with a spherical shape under the action of an external electromagnetic field. In contrast to the previous studies [2,22,53], we focus on other scenarios of collective resonances in subdiffraction arrays of dielectric nanospheres, namely, the Kerker lattice effect and quasi-BIC (Fig. 2). The discussion above shows the high capability of these resonances to control light behavior at the nanoscale. The advantage of incorporating spherical particles is that their optical response to an external plane wave and the examination of multipole coupling between them can be carried out analytically using Mie theory [6,57] and the Cartesian multipole moments [2,9] in the framework of a Green's tensor formalism [58]. Moreover, structures of spherical nanoparticles can be experimentally fabricated using laser ablation [59] or the technique of laser printing [60].

The paper is organized as follows. In Sec. II, we present an analytical system of coupled dipole equations that allows us to calculate electric and magnetic dipole moments of electromagnetically interacting nanoparticles. Then, the obtained dipole moments can be incorporated into expressions for the scattered field and radiated power of the array. In Sec. III, we investigate the properties of the lattice Kerker resonance that can be excited by a normally incident plane wave in finite-size nanoparticle arrays with a square unit cell [see Fig. 2(a)]. Emphasize that here we develop an approach that allows

us to obtain and tune the resonant lattice Kerker effect in finite-size metasurfaces with a square unit cell. In Sec. IV, we consider the excitation of quasi-BICs [Fig. 2(b)] in finite-size arrays by either an oblique incident plane wave or a point electric dipole. Essentially, in Secs. III and IV, we analyze the behavior of considered collective resonances by taking the number of particles forming the finite-size array (unit cells) as a degree of freedom. Additionally, we assess the applicability of the infinite-array theory in predicting the resonant response properties of finite-size arrays.

II. THEORETICAL MODEL

Through this work, we investigate the collective optical response of spherical nanoparticles with a diameter of 200 nm. The particles are made from crystalline silicon (c-Si), characterized by a dispersive dielectric permittivity [61]. The particles are arranged in periodic finite-size $N_{\text{tot}} \equiv N \times N$ arrays as shown in Fig. 2. The array has a square unit cell with the area $d \times d$, where d is the lattice period, such that $d < \lambda/n_S$ to avoid the diffraction of light. The particles are placed on a substrate made from quartz glass characterized by a refractive index of $n_S = \sqrt{\varepsilon_S} = 1.4$. The upper half space is assumed to be filled by a polymer characterized by the same refractive index $n_S = 1.4$. Such polymer can protect in experimental setups as the nanoparticle layer from damage [62].

The optical response of an isolated nanoparticle to a linearly polarized electromagnetic plane wave can be calculated using Mie theory, as described in Appendix A. Some details of the optical response are shown in Fig. 1. It is clear from the figure that the optical response of the nanoparticle in the considered spectral range (620–900 nm) is determined almost exclusively by scattering and it is associated only with the excitation of electric and magnetic dipoles. Therefore, an analytical model of coupled electric and magnetic dipole moments suffices to describe the optical response of finite-size nanoparticle arrays to an external field and the electromagnetic interaction between nanoparticles [2,63,64].

By employing a Green's tensor formalism, the electric $\mathbf{E}_{\text{dip}}(\mathbf{r}) = \mathbf{E}_p(\mathbf{r}) + \mathbf{E}_m(\mathbf{r})$ and magnetic $\mathbf{H}_{\text{dip}}(\mathbf{r}) = \mathbf{H}_p(\mathbf{r}) + \mathbf{H}_m(\mathbf{r})$ fields generated (scattered) by a collection of N_{tot} electric $(\mathbf{p}_1, \mathbf{p}_2, \mathbf{p}_3, \ldots, \mathbf{p}_{N_{\text{tot}}})$ and magnetic $(\mathbf{m}_1, \mathbf{m}_2, \mathbf{m}_3, \ldots, \mathbf{m}_{N_{\text{tot}}})$ dipole moments (or simple dipoles) at a point $\mathbf{r}$ read as

$$\begin{aligned}
\mathbf{E}_p(\mathbf{r}) &= \frac{k^2}{\varepsilon_0} \sum_{j=1}^{N_{\text{tot}}} \hat{\mathbf{G}}(\mathbf{r} - \mathbf{r}_j, \lambda)\mathbf{p}_j, \\
\mathbf{H}_p(\mathbf{r}) &= \frac{ck}{i} \sum_{j=1}^{N_{\text{tot}}} [\mathbf{g}(\mathbf{r} - \mathbf{r}_j, \lambda) \times \mathbf{p}_j], \\
\mathbf{E}_m(\mathbf{r}) &= \frac{ik}{c\varepsilon_0} \sum_{j=1}^{N_{\text{tot}}} [\mathbf{g}(\mathbf{r} - \mathbf{r}_j, \lambda) \times \mathbf{m}_j], \\
\mathbf{H}_m(\mathbf{r}) &= k_S^2 \sum_{j=1}^{N_{\text{tot}}} \hat{\mathbf{G}}(\mathbf{r} - \mathbf{r}_j, \lambda)\mathbf{m}_j,
\end{aligned} \tag{1}$$

where $\{\mathbf{r}_j\}_{j=1}^{N_{\text{tot}}}$ are positions of nanoparticles in the array, c is the vacuum light speed, ε_0 is the vacuum dielectric constant, $k_S = n_S k$ where k is the vacuum wave number related to the vacuum wavelength λ as $k = 2\pi/\lambda$, and $\times$ denotes the cross product [2]. Note that we omit the monochromatic time dependence $e^{-i\omega t}$ for compactness in the following text. $\hat{\mathbf{G}}(\mathbf{r} - \mathbf{r}_j, \lambda)$ is the electromagnetic Green's tensor for a point dipole source located at $\mathbf{r}_j$ while vector $\mathbf{g}$ is connected with the Green's tensor by the relationship $[\mathbf{g}(\mathbf{r} - \mathbf{r}_j, \lambda) \times \mathbf{p}_j] = \nabla \times \hat{\mathbf{G}}(\mathbf{r} - \mathbf{r}_j, \lambda)\mathbf{p}_j$, where the differentiation is carried out regarding $\mathbf{r}$ [65,66].

In the framework of coupled dipoles, the vectors of the electric dipole $\mathbf{p}_j$ and magnetic dipole $\mathbf{m}_j$ moments of spherical particle j with its center at $\mathbf{r}_j$ are determined by the local electric $\mathbf{E}_{\text{loc}}(\mathbf{r}_j)$ or magnetic $\mathbf{H}_{\text{loc}}(\mathbf{r}_j)$ field acting on the particle [2]

$$\mathbf{p}_j = \alpha_p(\lambda)\mathbf{E}_{\text{loc}}(\mathbf{r}_j), \quad \mathbf{m}_j = \alpha_m(\lambda)\mathbf{H}_{\text{loc}}(\mathbf{r}_j). \tag{2}$$

For a spherical nanoparticle, wavelength-dependent electric α_p and magnetic α_m dipole polarizabilities are expressed as analytical scalar functions using Mie theory [see Eq. (A3) in Appendix A].

In the case of a single particle, the local fields in Eq. (2) are the electric $\mathbf{E}_{\text{inc}}(\mathbf{r}_j)$ and magnetic $\mathbf{H}_{\text{inc}}(\mathbf{r}_j)$ fields of the incident plane wave.

For a nanoparticle in the array, the local electric $\mathbf{E}_{\text{loc}}(\mathbf{r}_j)$ [respectively magnetic $\mathbf{H}_{\text{loc}}(\mathbf{r}_j)$] field acting on particle j is a superposition of three contributions:

(1) the incident electric field $\mathbf{E}_{\text{inc}}(\mathbf{r}_j)$ [respectively magnetic field $\mathbf{H}_{\text{inc}}(\mathbf{r}_j)$],

(2) the electric field $\mathbf{E}'_p(\mathbf{r}_j)$ [respectively magnetic field $\mathbf{H}'_p(\mathbf{r}_j)$] generated by electric dipoles of all particles except jth one, and

(3) the electric field $\mathbf{E}'_m(\mathbf{r}_j)$ [respectively magnetic field $\mathbf{H}'_m(\mathbf{r}_j)$] generated by magnetic dipoles of all particles except jth one.

The primed fields can be obtained from Eq. (1) by excluding the terms with $\mathbf{p}_j$ and $\mathbf{m}_j$. According to Eq. (2), we obtain a linear system of $6N_{\text{tot}}$ coupled dipole equations:

$$\begin{aligned}
\mathbf{p}_j &= \alpha_p \mathbf{E}_{\text{inc}}(\mathbf{r}_j) + \alpha_p \frac{k^2}{\varepsilon_0} \sum_{\substack{l=1 \\ l \neq j}}^{N_{\text{tot}}} \hat{\mathbf{G}}(\mathbf{r}_j - \mathbf{r}_l, \lambda)\mathbf{p}_l \\
&\quad + \alpha_p \frac{ik}{c\varepsilon_0} \sum_{\substack{l=1 \\ l \neq j}}^{N_{\text{tot}}} [\mathbf{g}(\mathbf{r}_j - \mathbf{r}_l, \lambda) \times \mathbf{m}_l], \\
\mathbf{m}_j &= \alpha_m \mathbf{H}_{\text{inc}}(\mathbf{r}_j) + \alpha_m k_S^2 \sum_{\substack{l=1 \\ l \neq j}}^{N_{\text{tot}}} \hat{\mathbf{G}}(\mathbf{r}_j - \mathbf{r}_l, \lambda)\mathbf{m}_l \\
&\quad + \alpha_m \frac{ck}{i} \sum_{\substack{l=1 \\ l \neq j}}^{N_{\text{tot}}} [\mathbf{g}(\mathbf{r}_j - \mathbf{r}_l, \lambda) \times \mathbf{p}_l].
\end{aligned} \tag{3}$$

After the solution of this system, the total scattered field can be calculated as a superposition of fields (1) generated by all electric and magnetic dipoles in the array. The far-field scattered power $dP_{\text{sca}} = \langle \mathbf{S} \rangle \cdot \mathbf{n} r^2 \, d\Omega$ into the solid angle $d\Omega = \sin\theta \, d\theta \, d\varphi$ is determined by the time-averaged Poynting vector such that $\langle \mathbf{S} \rangle = 1/2 \, \text{Re}[\mathbf{E}_{\text{FF}} \times$

$\mathbf{H}_{\mathrm{FF}}^{*}] = 1/2\sqrt{\varepsilon_0\varepsilon_S/\mu_0}|\mathbf{E}_{\mathrm{FF}}|^2\mathbf{n}$, where $\mathbf{E}_{\mathrm{FF}}$ and $\mathbf{H}_{\mathrm{FF}}$ are the contributions of the fields in Eq. (1) in the far field. Let us introduce the so-called *radiation pattern* as $f(\mathbf{n}) = 1/2\sqrt{\varepsilon_0\varepsilon_S/\mu_0}r^2|\mathbf{E}_{\mathrm{FF}}|^2$, which can be written in the dipole approximation as [67]

$$f(\mathbf{n}) = \frac{1}{2}\sqrt{\frac{\varepsilon_0\varepsilon_S}{\mu_0}}\frac{k_S^4}{16\pi^2\varepsilon_0^2\varepsilon_S^2} \times \left|\sum_{j=1}^{N_{\mathrm{tot}}} e^{-ik_S(\mathbf{n}\cdot\mathbf{r}_j)}\left([\mathbf{p}_j - (\mathbf{n}\cdot\mathbf{p}_j)\mathbf{n}] + \frac{1}{c_S}\mathbf{m}_j\times\mathbf{n}\right)\right|^2, \tag{4}$$

where $\mathbf{n} = (\sin\theta\,\cos\varphi, \sin\theta\,\sin\varphi, \cos\theta)$ is a normal vector to a spherical surface, $c_S = c/n_S$ is the light speed in the medium with n_S.

A total scattered power is an integral of the radiation pattern over a spherical surface:

$$P_{\mathrm{sca}} = \int_0^{2\pi} d\varphi \int_0^{\pi} d\theta\,\sin\theta f(\mathbf{n}). \tag{5}$$

The scattering cross section for an incident plane wave with intensity $I_{\mathrm{inc}} = 1/2\sqrt{\varepsilon_0\varepsilon_S/\mu_0}|\mathbf{E}_{\mathrm{inc}}|^2$ is defined as $\sigma_{\mathrm{sca}} = P_{\mathrm{sca}}/I_{\mathrm{inc}}$, which reads as in the dipole approximation

$$\sigma_{\mathrm{sca}} = \frac{k_S^4}{16\pi^2\varepsilon_0^2\varepsilon_S^2|\mathbf{E}_{\mathrm{inc}}|^2}\int_0^{2\pi} d\varphi\int_0^{\pi} d\theta\,\sin\theta \times \left|\sum_{j=1}^{N_{\mathrm{tot}}} e^{-ik_S(\mathbf{n}\cdot\mathbf{r}_j)}\left([\mathbf{p}_j - (\mathbf{n}\cdot\mathbf{p}_j)\mathbf{n}] + \frac{1}{c_S}\mathbf{m}_j\times\mathbf{n}\right)\right|^2. \tag{6}$$

III. DEVELOPMENT OF RESONANT KERKER EFFECT IN FINITE-SIZE ARRAYS

The collective effects of electromagnetic coupling between particles can strongly modify their response compared to the single-particle case. To numerically evaluate the optical response of finite-size nanoparticle arrays, we apply the outlined theoretical model based on the coupled dipole approximation (see Sec. II). However, it is natural to consider also the collective resonances for infinite arrays, *lattices,* since the analysis of the systems with ideal translational symmetry can be carried out analytically using the lattice sum approach as described in detail in Appendix B. This analysis can help us obtain analytical conditions for the lattice Kerker and quasi-BIC resonances, further verified for the finite-size arrays. These conditions provide us with the lattice period for a given operating wavelength to observe these resonances.

Let us obtain a condition of the resonant lattice Kerker effect in an infinite square array and consider a normally incident ($\mathbf{k} = k_S\mathbf{e}_z$) plane wave with field components $\mathbf{E}_{\mathrm{inc}}(\mathbf{r}) = E_{\mathrm{inc}}e^{ik_Sz}\mathbf{e}_x$ and $\mathbf{H}_{\mathrm{inc}}(\mathbf{r}) = H_{\mathrm{inc}}e^{ik_Sz}\mathbf{e}_y$ where $H_{\mathrm{inc}} = E_{\mathrm{inc}}\sqrt{\varepsilon_0\varepsilon_S/\mu_0}$. According to Eq. (2), this plane wave excites in-plane components of dipole moments $p_x = \alpha_pE_{\mathrm{inc}}$ and $m_y = \alpha_mH_{\mathrm{inc}}$ in a single particle. For the infinite square array, the electric dipole (ED) and magnetic dipole (MD) components induced in each nanoparticle can be expressed via external fields and so-called effective polarizabilities [see Eq. (B1) in Appendix B]:

$$p_{0,x} = \frac{\varepsilon_0\varepsilon_SE_{\mathrm{inc}}}{\varepsilon_0\varepsilon_S/\alpha_p - S_{\parallel}}, \quad m_{0,y} = \frac{H_{\mathrm{inc}}}{1/\alpha_m - S_{\parallel}}, \tag{7}$$

where $S_{\parallel}$ is the so-called lattice sum given by Eq. (B3) in Appendix B (the subscript $\parallel$ indicates the in-plane orientation of dipoles). The lattice sum considers the electromagnetic coupling between nanoparticles. Note that for a lattice of spherical nanoparticles with a square unit cell under a normally incident plane wave illumination, electric and magnetic dipoles of nanoparticles are uncoupled and can be considered independently.

Moreover, a square lattice with period $d < \lambda/n_S$ and illuminated by a normally incident plane wave can radiate only in vertical $\pm z$ directions with the amplitude and phase given by the radiation pattern of the unit cell (spherical nanoparticle, in our case):

$$f_{\mathrm{array}}(\mathbf{n} = \pm\mathbf{e}_z) \propto f_{\mathrm{particle}}(\mathbf{n} = \pm\mathbf{e}_z) \propto \left|\mathbf{e}_x\left(p_{0,x} \pm \frac{m_{0,y}}{c_S}\right) + \mathbf{e}_y\left(p_{0,y} \mp \frac{m_{0,x}}{c_S}\right)\right|^2. \tag{8}$$

The amplitude $f_{\mathrm{particle}}(\mathbf{n} = +\mathbf{e}_z)$ gives a contribution to the transmission of the array, while $f_{\mathrm{particle}}(\mathbf{n} = -\mathbf{e}_z)$ determines the reflection. The derivation of Eq. (8) is provided in Appendix B. We would note that Eq. (8) can be extended beyond the dipole approximation by adding components of higher-order multipole tensors that can be excited by a transverse electric (TE) or transverse magnetic (TM) polarized plane wave; for the details, please see Eqs. (13)– (16) in Ref. [20].

For a single dipole nanoparticle, the Kerker condition is $\alpha_p/\varepsilon_0\varepsilon_S = \alpha_m$ or $a_1 = b_1$ in Eq. (A3) [68]. Then, $p_x = m_y/c$ that results in the suppression of plane-wave scattering in the backward direction, i.e., $f_{\mathrm{particle}}(\mathbf{n} = -\mathbf{e}_z) = 0$ according to Eq. (8), known as the Kerker effect. For the considered isolated silicon nanoparticle, the nonresonant Kerker effect can be observed for $\lambda_K = 834$ nm in Fig. 1.

However, with the nanosphere array, one can obtain at the same $\lambda_K = 834$ nm the resonant Kerker effect, which is the suppression of the backward-scattered waves and the overall reflection from the array at the resonant values of electric $\mathbf{p}_0$ and magnetic $\mathbf{m}_0$ dipole moments, i.e., $f_{\mathrm{array}}(\mathbf{n} = -\mathbf{e}_z) = 0$ in Eq. (8) [37]. To achieve this, we developed the following strategy. We need to adjust the spectral positions of lattice ED and MD resonances at the wavelength λ_K. The collective resonances in the array response appear when the real parts of denominators of effective lattice polarizabilities equal zero. For in-plane induced dipoles, the effective electric $\alpha_p^{(\mathrm{eff})}$ and magnetic $\alpha_m^{(\mathrm{eff})}$ polarizabilities for particles in the infinite array can be extracted from Eq. (7) as

$$\alpha_p^{(\mathrm{eff})} = \left(\frac{\varepsilon_0\varepsilon_S}{\alpha_p} - S_{\parallel}\right)^{-1}, \quad \alpha_m^{(\mathrm{eff})} = \left(\frac{1}{\alpha_m} - S_{\parallel}\right)^{-1}. \tag{9}$$

The effective polarizabilities provide us with analytical conditions for the resonant Kerker effect in the infinite array (lattice) within the dipole approximation and they read as

$$\alpha_p^{(\mathrm{eff})} = \alpha_m^{(\mathrm{eff})}, \quad \mathrm{Re}\left[1/\alpha_p^{(\mathrm{eff})}\right] = \mathrm{Re}\left[1/\alpha_m^{(\mathrm{eff})}\right] = 0. \tag{10}$$

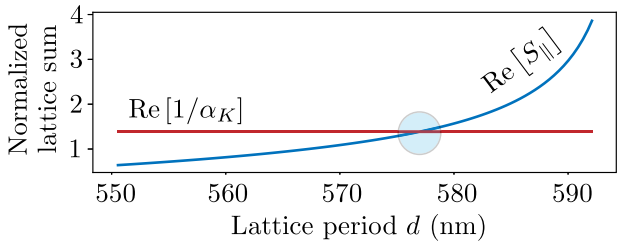

FIG. 3. Numerically evaluated lattice sum for in-plane (∥) dipoles (blue) and the real part of the inverse single-particle dipole polarizabilities (red) as a function of the lattice period $d < \lambda_K/n_S$ at the Kerker wavelength $\lambda_K = 834$ nm (see Fig. 1). The quantities are normalized by $6\pi/k_S^3$. The blue circle indicates the lattice period such that the ED and MD lattice resonances overlap, and the lattice resonant Kerker effect emerges according to Eq. (10).

Since the electric field reflection coefficient $r \propto [\alpha_p^{(\mathrm{eff})} - \alpha_m^{(\mathrm{eff})}]$ [2], the first condition in Eq. (10) guarantees the emergence of the Kerker effect. In contrast, the second one is the condition for the ED and MD resonances to occur in the lattice at the same wavelength. Note that the lattice Kerker effect conditions in Eq. (10) are valid for arrays with any unit cell. Moreover, considering the response of higher-order multipole moments, Eq. (10) can be modified by splitting multipole moments into two sets with opposite parity inversion using the methodology from Ref. [69].

Let us consider Eq. (10) for square arrays of spherical nanoparticles. According to Eq. (A4) and Fig. 11, $\varepsilon_0\varepsilon_S/\alpha_p = 1/\alpha_m \equiv 1/\alpha_K$ at $\lambda_K = 834$ nm that corresponds to the Kerker effect for isolated particles in our case (Fig. 1). Then the first condition in Eq. (10) is automatically satisfied at this wavelength since the lattice sum $S_\parallel$ for the electric and magnetic dipole subsystems coincides. Note that the value of α_K lies beyond the single-particle dipole resonances on the side of long wavelengths. Furthermore, the second condition in Eq. (10), using Eq. (9), transforms to the following lattice resonant condition:

$$\mathrm{Re}[1/\alpha_K] = \mathrm{Re}[S_\parallel]. \tag{11}$$

This condition can be used to determine the lattice period d at which the corresponding lattice resonance coincides with the Kerker effect at $\lambda_K = 834$ nm. In contrast to the imaginary part of lattice sum $\mathrm{Im}[S_\parallel]$ [see Eq. (B4)], its real part $\mathrm{Re}[S_\parallel]$ is slowly converging. Therefore, it cannot be calculated analytically but should be evaluated numerically. Here, we employ the effective Ewald's summation method [70] implemented in TREAMS [71]. The results of the $\mathrm{Re}[S_\parallel]$ calculation are given in Fig. 3 as a function of the period d at the fixed $\lambda_K = 834$ nm. In Fig. 3, the value $\mathrm{Re}[1/\alpha_K]$ is also presented. One can find that lattice period $d = 577$ nm obeys the condition in Eq. (11) for the resonant lattice Kerker effect. Indeed, for the lattice with $d = 577$ nm, both $\alpha_p^{(\mathrm{eff})}$ and $\alpha_m^{(\mathrm{eff})}$ polarizabilities [Eq. (9)] have a resonance at the wavelength $\lambda_K = 834$ nm. This is clearly visible from the coincidence of resonances in Fig. 4(a).

For the infinite array, we can introduce an effective scattering cross section per particle $\sigma_{0,\mathrm{eff}}$ that can be calculated via Eq. (A5) by replacing the single-particle polarizabilities with effective ones (9), $\alpha_p \to \varepsilon_0\varepsilon_S\alpha_p^{(\mathrm{eff})}$ and $\alpha_m \to \alpha_m^{(\mathrm{eff})}$. The

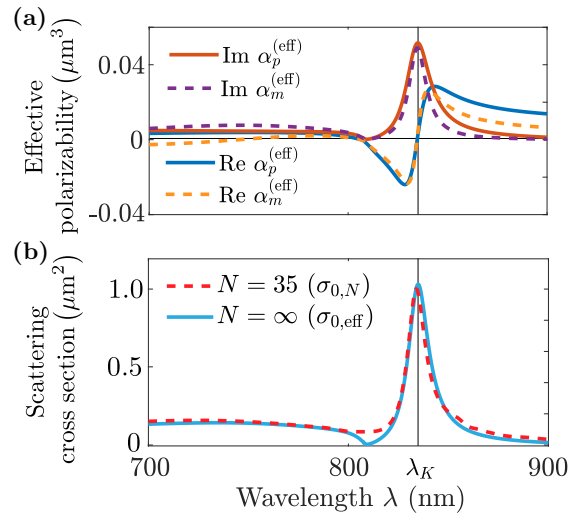

FIG. 4. (a) Effective ED and MD polarizabilities of a nanoparticle in the infinite square lattice for in-plane dipoles (9) as a function of wavelength of normally incident plane wave. (b) Scattering cross section per particle σ_0 for (blue) the infinite and (red dashed) 35×35 particle array. The values of the wavelength λ are indicated for vacuum.

effective cross section $\sigma_{0,\mathrm{eff}}$ for the lattice with $d = 577$ nm has a resonance at the wavelength λ_K, indicating the resonant lattice Kerker effect. The resonance has a quality factor $Q_\infty \approx 70$. Here, the Q factor is defined as $Q = \lambda/\Delta\lambda$ where λ is the resonant wavelength and $\Delta\lambda$ is the full width at half-maximum.

Due to a lack of translational symmetry, the lattice sum approach does not apply to a finite array to calculate the dipole moments. Therefore, we will solve a system of coupled dipole equations (3) numerically using MATLAB. In this model, each nanoparticle is characterized by three components of the ED moment (p_x, p_y, p_z) and three components of the MD moment (m_x, m_y, m_z), depending on the ED and MD moments of all the other nanoparticles via the coupling in free space governed by Green's functions. Thus, for the array of $N \times N$ particles, we need to solve a system of $6 \times N^2$ linear equations. Further, the calculated dipole moments can be incorporated into Eq. (6) to calculate the total scattering cross section σ_{sca}. For the finite array, we can also formally define the scattering cross section per particle as $\sigma_{0,N} = \sigma_{\mathrm{sca}}/N^2$.

The application of this approach to the arrays with a finite number of particles showed that, already for the 35×35 array, there is a good coincidence of the array's resonant response with the infinite array case [see Fig. 4(b)]. A single exception is behavior at the wavelength of 808 nm where the scattering of the infinite array is eliminated. This is the wavelength of the so-called Rayleigh-Wood anomaly [72,73] when the lattice period equals the wavelength of incident light in the surrounding medium $d = \lambda/n_S$. In our case with $d = 577$ nm and $n_S = 1.4$, this leads to $\lambda = dn_S \approx 808$ nm in vacuum. This wavelength corresponds to the singularity of lattice sums (B3) that occur in the denominators of induced dipole moments (2). When it happens that $p_{0,x} = m_{0,y} = 0$, the incident light is fully transmitted. In that case, we can speak of an electromagnetically induced transparency (EIT),

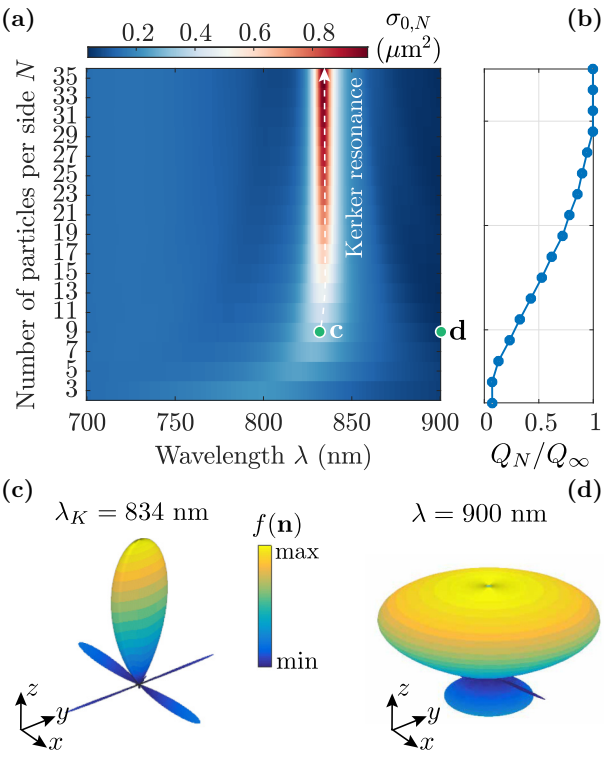

FIG. 5. (a) Scattering cross section per particle $\sigma_{0,N} \equiv \sigma_{\text{sca}}(N)/N^2$, where $\sigma_{\text{sca}}(N)$ is the total scattering cross section (6) for the $N \times N$ array with lattice period $d = 577$ nm. The array is illuminated by an external plane wave as shown in Fig. 3. The green points, labeled c and d, indicate N and λ for which the radiation patterns are plotted in (c) and (d), respectively. (b) The quality factor of the collective Kerker resonance as a function of N, which is normalized by the quality factor for the infinite lattice $Q_\infty = 70$ calculated via Fig. 4(b). (c) Far-field radiation pattern, given by Eq. (4), for the 9×9 array with lattice period $d = 577$ nm at the Kerker wavelength $\lambda_K = 834$ nm. (d) The same but at the wavelength $\lambda = 900$ nm, which is far from resonances. The values of the wavelength λ are indicated for vacuum.

something that occurs exclusively because of a long-range coupling in the infinite lattice. However, in contrast to the lattice Kerker effect, the EIT cannot be observed in small-size finite arrays for the resonant enhancement of transmitted light [see Fig. 4(b)] since the interaction length in finite arrays is limited by relatively small array boundaries.

Figure 5(a) shows the development of the resonant Kerker effect for arrays with different numbers of particles per side of the array. In this figure, the (N, λ) map of $\sigma_{0,N}$ is presented for the array with period $d = 577$ nm predicted. One can see that the lattice Kerker resonance becomes pronounced in the finite array with a relatively small number of particles $N \approx 9$ per side. The spectral position of the lattice Kerker effect in the finite-size array converges to that in the infinite array $\lambda = 834$ nm for $N \gtrsim 15$ [see Fig. 5(a)]. As the number of particles N increases, the resonance becomes more and more noticeable, with the resonant value of $\sigma_{0,N}(\lambda_K)$ approaching the limit of the infinite array $\sigma_{0,\text{eff}}(\lambda_K) = 1$ μm^2 for $N \gtrsim 30$. Note that the in-plane disorder of nanoparticle positions influences only the cross-section amplitude at the resonance, keeping the qualitative behavior as shown in Appendix D. Moreover, the Q factor of the resonance in the finite array Q_N also saturates at the value of the infinite array Q factor for an array larger than 29×29 as shown in Fig. 5(b). Thus, the characteristics of the resonant Kerker effect converge to the infinite array limit for about 30×30 particles.

Figure 5 also shows the radiation pattern $f(\mathbf{n})$ for the 9×9 array calculated using Eq. (4). One can see in Fig. 5(c) that the array mainly radiates in the forward direction regarding the incident light, i.e., $z > 0$ direction, at the Kerker resonance wavelength in contrast to the nonresonant case shown in Fig. 5(d). However, Fig. 5(c) also demonstrates low-amplitude radiation lobes in the array plane that appear due to the finite size of the array. As the array size increases, their amplitude tends to zero.

In this section, we first employed the lattice sum method to predict the lattice period for which the resonant lattice Kerker effect can be observed at wavelengths such that the Kerker effect condition is satisfied for a single particle. We also investigated this effect in finite arrays with the lattice period obtained for the infinite lattice. Figure 5 can be used to choose the array size to realize the resonant response of the array to the normally incident plane wave with the desired amplitude and quality factor. Note that, using the developed approach, one can easily tune the resonant Kerker effect to the desired spectral position by selecting the size of the silicon particles or their material which control the value of λ_K and determining the required lattice period by using Eq. (11).

IV. DEVELOPMENT OF QUASI-BIC RESPONSE IN FINITE-SIZE ARRAYS

This section considers another collective effect that emerges due to dipole coupling between nanoparticles. According to expressions for a spherical nanoparticle's ED and MD moments in the infinite lattice (B1), a normally incident plane wave can excite only in-plane components of dipole moments. Let us consider a case of a lattice eigenmode with out-of-plane ED or MD moments of nanoparticles ($p_{0,z}$ or $m_{0,z}$) being all the moments are in phase (Γ point of the Brillouin zone). According to Eq. (8), the infinite lattice in the subdiffraction limit can radiate power into the far field only along its normal direction, i.e., z axis. The lattice can radiate if nanoparticles have in-plane components of their dipole moments. However, electric and magnetic dipoles do not radiate along their axes. Therefore, a collective state polarized along the lattice normal (z axis) is a nonradiant one. Hence, such a state can generate fields concentrated only in the near field of the lattice, and they are called symmetry-protected (Γ-point) bound states in the continuum [19,40]. Because of the reciprocity theorem [74], bound states in the continuum cannot be excited by propagating plane waves. Note that, in the general case, multipole decompositions of symmetry-protected BICs contain only multipoles that do not radiate along the lattice normal (z axis) [75,76].

A. Excitation from the far field

Let us focus on the magnetic dipole bound state in the continuum (BIC). Note that eigenfrequencies of BICs for the

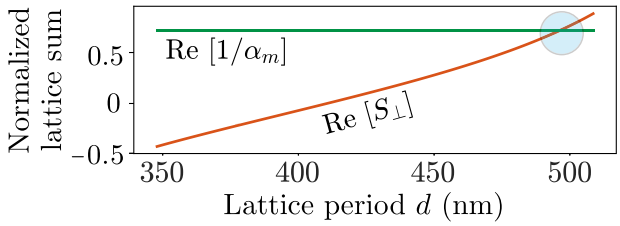

FIG. 6. Numerically evaluated real part of lattice sum for out-of-plane ($\perp$) dipoles (red), and the real part of the inverse single-particle MD polarizability (green) as a function of lattice period $d < \lambda/n_S$ at the wavelength $\lambda = 808$ nm. The quantities are normalized by $6\pi/k_S^3$. The blue circle indicates the lattice period such that the lattice supports a magnetic dipole BIC according to Eq. (C1).

infinite lattice of nonabsorbing particles are real since the states are free of radiative losses. In the considered spectral range 620–900 nm, silicon has low absorption. This can be seen from the results shown in Fig. 1, where the scattering cross section nearly makes up the entire extinction cross section. Therefore, we can select a real operating wavelength to exploit such a mode and then find the lattice period satisfying Eq. (C2) that enables the presence of this mode within the corresponding array. Let us choose $\lambda = 808$ nm to spectrally separate MD resonance in the single particle at $\lambda \approx 775$ nm and magnetic BIC resonance of a lattice. Please remember that we consider silicon nanoparticles with a diameter of 200 nm, shown in Fig. 1. For the real parts of the inverse single-particle MD polarizability and the lattice sum for the out-of-plane dipoles [see Eq. (B3)] evaluated at this wavelength, we need to find their crossing point according to Eq. (C2) in Appendix C. As follows from Fig. 6, an array with a period of $d = 495$ nm will support the magnetic dipole BIC at $\lambda = 808$ nm.

In infinite lattices, the radiative losses of BICs are nullified due to the interaction between an infinite number of unit cells. Consequently, finite-size nanoparticle arrays cannot truly support BICs with an infinitely large radiative Q factor. However, they can support quasi-BICs characterized by narrow resonances of Fano type in the scattering spectrum [77]. Unlike the ideal scenario of BICs, quasi-BICs can possess a large but finite radiative Q factor and can be excited by external electromagnetic fields in compliance with the reciprocity theorem [74]. To excite out-of-plane MD component (m_z) for particles in a finite-size array, we employ an oblique incident plane wave with wave vector $\mathbf{k} = k_S \sin(\theta_{\rm inc})\mathbf{e}_x + k_S \cos(\theta_{\rm inc})\mathbf{e}_z$, electric field $\mathbf{E}_{\rm inc}(\mathbf{r}) = E_{\rm inc} e^{i\mathbf{k}\cdot\mathbf{r}}\mathbf{e}_y$, and magnetic field $\mathbf{H}_{\rm inc}(\mathbf{r}) = H_{\rm inc} e^{i\mathbf{k}\cdot\mathbf{r}}[-\cos(\theta_{\rm inc})\mathbf{e}_x + \sin(\theta_{\rm inc})\mathbf{e}_z]$ as illustrated by the inset in Fig. 7(a). Note that, for the BIC, there is no phase shift $e^{ik_S \sin(\theta_{\rm inc})x}$ between m_z components of particles. Therefore, we choose a relatively small angle of incidence $\theta_{\rm inc} = 2^\circ$. On the other hand, the incident wave still contains field component H_z that induces an out-of-plane (m_z) component of the MD moment in each nanoparticle. The out-of-plane component allows us to observe a resonant response associated with the magnetic quasi-BIC.

Figure 7(a) shows that the 13×13 array with lattice period $d = 495$ nm, obtained for the infinite lattice, exhibits a narrow resonance in the mean value of the out-of-plane MD

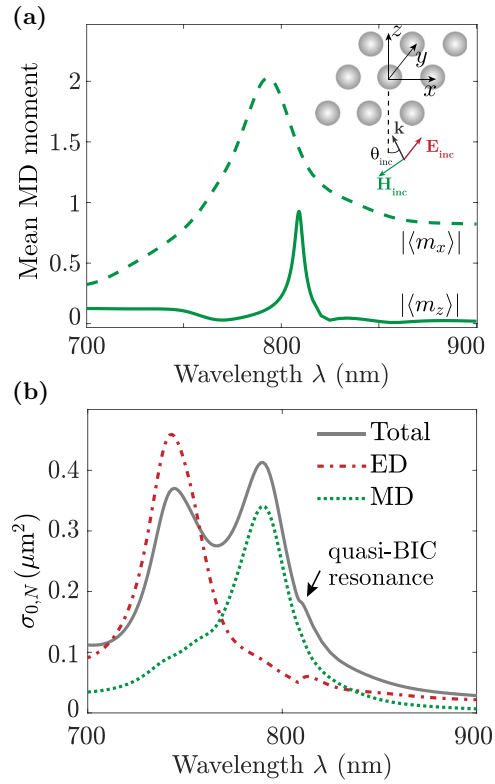

FIG. 7. Magnetic dipole quasi-BIC resonance in the finite-size array of 13×13 particles with period $d = 495$ nm. (a) Mean values $|\langle m_x \rangle|$ (dashed) and $|\langle m_z \rangle|$ (solid) of MD components [Eq. (12)] that can be induced by an oblique incident plane wave with the polarization shown by the inset. The components are normalized by $|\alpha_m \mathbf{H}_{\rm inc}|$. The angle of incidence is $\theta_{\rm inc} = 2^\circ$. (b) Total scattering cross section (6) per particle $\sigma_{0,N} \equiv \sigma_{\rm sca}(N)/N^2$ (gray solid), and independent contributions of EDs and MDs to the scattering per particle (red dashed-dotted and green dotted, respectively). The values of the wavelength λ are indicated for vacuum.

moment component $|\langle m_z \rangle|$ at $\lambda = 808$ nm, and a broad resonance in the mean value of the in-plane component $|\langle m_x \rangle|$ at $\lambda \approx 775$ nm. The mean value of MD moments is defined as

$$\langle \mathbf{m} \rangle = \frac{1}{N_{\rm tot}} \sum_{j=1}^{N_{\rm tot}} \mathbf{m}_j. \tag{12}$$

The broad resonance of $|\langle m_x \rangle|$ originates from the single-particle MD resonance. The narrow resonance of $|\langle m_z \rangle|$ emerges due to the excitation of collective quasi-BIC. The latter manifests in a spectral feature in the scattering cross section [Fig. 7(b)] that is not observed for a single particle (Fig. 1).

Figure 8 shows the amplitude of the mean value $|\langle m_z \rangle|$ as a function of particle number N and wavelength λ for an oblique incident plane wave. One can see that the spectral position of the $|\langle m_z \rangle|$ resonance converges to that for the infinite lattice at $\lambda = 808$ nm as particle number N increases. The appearance of the maximum of the resonant value of $|\langle m_z \rangle|/|\alpha_m \mathbf{H}_{\rm inc}| \approx 1.2$ for $N \approx 21$ testifies about the constructive interference between the incident and the scattered fields. Although the resonant value of $|\langle m_z \rangle|$ has a nonmonotonic dependence on N, the Q factor of the quasi-BIC resonance rather increases

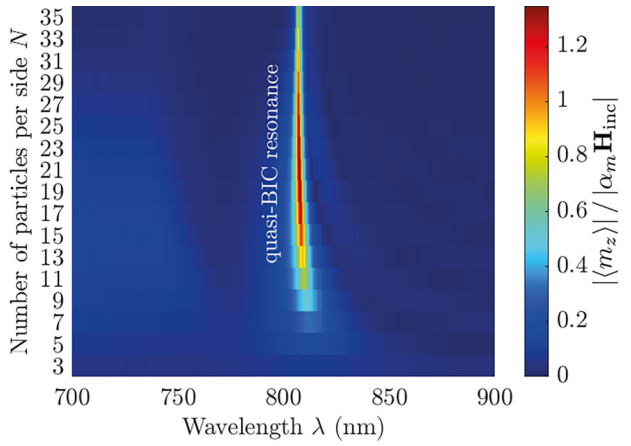

FIG. 8. Mean value $|\langle m_z\rangle|$ of the out-of-plane MD component, given by Eq. (12), that is induced by an oblique incident plane wave with the polarization as shown by the inset in Fig. 7(a). The angle of incidence is $\theta_{\text{inc}} = 2^\circ$. The $N \times N$ array has a lattice period of $d = 495$ nm. The resonant phenomenon is associated with the excitation of magnetic dipole quasi-BIC in the finite array of nanoparticles. The values of the wavelength λ are indicated for vacuum.

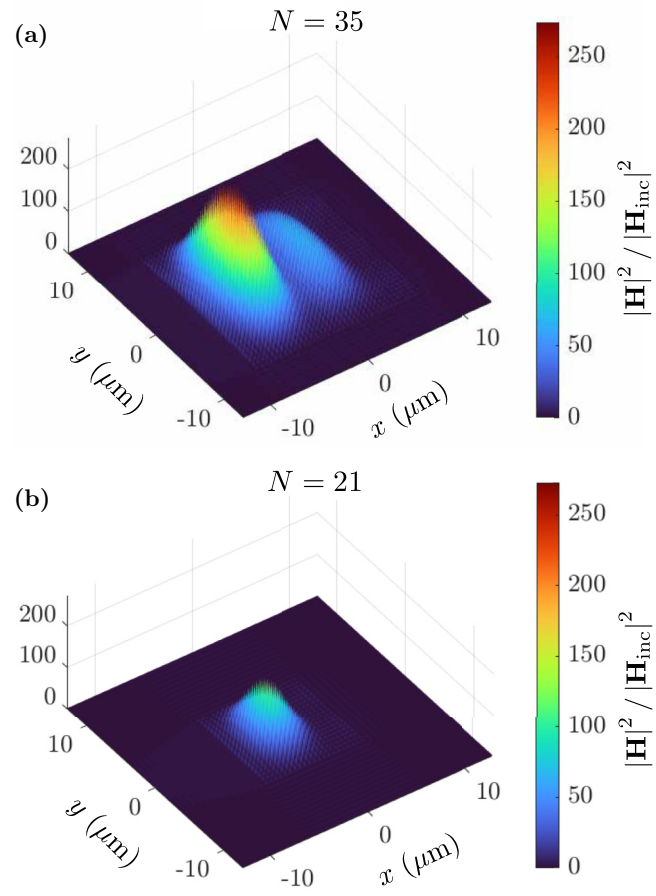

FIG. 9. Normalized magnetic energy density determined by the total magnetic field in the xy plane at position $z = 110$ nm above the array. The array has (a) 35×35 particles and (b) 21×21 particles. An oblique incident plane wave, shown by the inset in Fig. 7(a), has a wavelength of the resonant magnetic dipole quasi-BIC excitation $\lambda = 808$ nm.

with N and saturates for $N \gtrsim 30$ as shown in Fig. 13(a) (details on the calculation of the Q factor of the quasi-BIC are presented in Appendix E). Indeed, the inverse total Q factor of the quasi-BIC can be written as $Q_{\text{tot}}^{-1} = Q_{\text{rad}}^{-1} + Q_{\text{abs}}^{-1}$ where Q_{rad} and Q_{abs} are the radiative and nonradiative contributions to the Q factor. Although, $Q_{\text{rad}}^{-1} \to 0$ for $N \to \infty$, the total Q factor is limited by Q_{abs} for finite and infinite arrays due to the presence of intrinsic absorption losses in particles. The value of Q_{abs} can be approximated as $\text{Re}(\varepsilon)/\text{Im}(\varepsilon)$ where the silicon dielectric permitivitty ε should be taken at the resonance wavelength $\lambda = 808$ nm [55]. If we artificially nullify the material losses by setting $\text{Im}(\varepsilon) \equiv 0$, the Q factor will be larger and increase with N as shown in Fig. 13(a). Moreover, the calculations show that, in the absence of material losses, the resonant value of $|\langle m_z\rangle|/|\alpha_m \mathbf{H}_{\text{inc}}|$ increases with N and reaches ≈ 6 for $N = 35$. Thus, engineering of material losses, as, e.g., in Ref. [78], is important for reaching large Q factors of quasi-BICs.

Taking back the material losses of silicon, we also calculate the Q factor for various angles of incidence θ_{inc} of an external plane wave. As the angle increases, the phase shift $e^{ik_S \sin(\theta_{\text{inc}})x}$ between induced magnetic dipole moments in particles becomes larger resulting in the fast reduction of Q factor [see Fig. 13(b)], being in agreement with the results for BIC in infinite arrays [55,79]. Moreover, one can observe the oscillations of Q factor caused by the interference between incident and scattered fields.

As mentioned above, high-Q quasi-BICs weakly radiate into the far field, resulting in a concentration of electromagnetic fields near the structure. Figure 9 shows distributions of the normalized magnetic energy density determined by the total magnetic field $\mathbf{H}(\mathbf{r}) = \mathbf{H}_{\text{inc}}(\mathbf{r}) + \mathbf{H}_p(\mathbf{r}) + \mathbf{H}_m(\mathbf{r})$, where $\mathbf{H}_p(\mathbf{r})$ and $\mathbf{H}_m(\mathbf{r})$ are the magnetic fields generated by electric and magnetic dipoles of nanoparticles in the array, respectively [Eq. (1)]. The fields are calculated in the $z = 110$ nm plane, where the particle radius is 100 nm. It can be seen that the magnetic field in the near field is significantly enhanced compared to the incident field at the wavelength of magnetic dipole quasi-BIC resonance. Moreover, the array with $N = 21$ provides a more homogeneous distribution of the near magnetic field than the array with $N = 35$, but with a lower amplitude. As discussed above, this is observed due to the boundary effects.

B. Excitation from the near field

The above approach can also be applied to excite an electric dipole quasi-BIC in a finite-size array from the far field using an oblique incident plane wave with E_z component. However, we additionally consider here the electric dipole quasi-BIC excitation from the near field employing an electric dipole $\mathbf{p}_{\text{inc}}$, which generates incident electric field $\mathbf{E}_{\text{inc}}(\mathbf{r}) = k^2/\varepsilon_0 \hat{\mathbf{G}}(\mathbf{r} - \mathbf{r}', \lambda)\mathbf{p}_{\text{inc}}$ and magnetic field $\mathbf{H}_{\text{inc}}(\mathbf{r}) = -ick\mathbf{g}(\mathbf{r} - \mathbf{r}', \lambda) \times \mathbf{p}_{\text{inc}}$. As shown by the inset in Fig. 10(a), the electric dipole is placed above the array at the position $\mathbf{r}' = g\mathbf{e}_z$ where we put $g = 150$ nm. Unlike a plane wave, an electric dipole generates a strong electric near field that can couple to an electric field of the electric dipole quasi-BIC

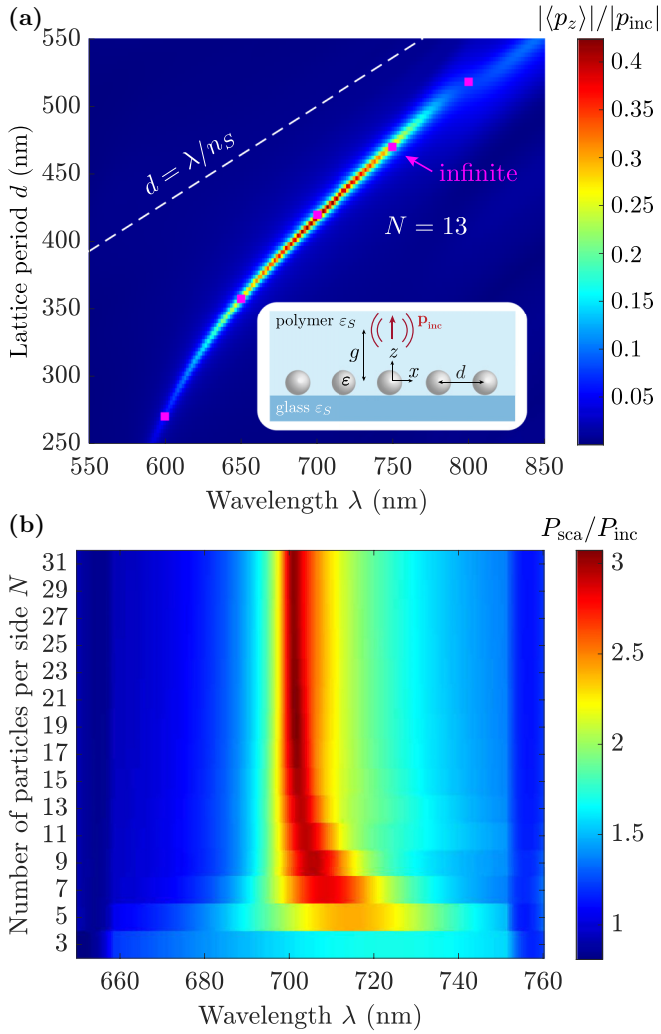

FIG. 10. (a) Mean value $|\langle p_z\rangle|$ of the out-of-plane ED component induced from the near field by an electric dipole $\mathbf{p}_{\rm inc}$ as shown in the inset. The electric dipole is placed at $g = 150$ nm above the 13×13 array. The pink markers indicate the pairs of parameters (d, λ), which obey Eq. (C1) corresponding to the electric dipole BIC observation in the infinite array. (b) Total scattered power (5) for the $N \times N$ array with lattice period $d = 423$ nm as a function of N and wavelength of incident dipole radiation. The power $P_{\rm sca}$ is normalized by the power of the incident dipole radiation $P_{\rm inc} = \frac{4\pi^3|\mathbf{p}_{\rm inc}|^2}{3\varepsilon_0^2 c_S \mu_0 \lambda^4}$ where μ_0 is the vacuum magnetic permeability [9]. The values of the wavelength λ are indicated for vacuum.

that is primarily localized in the near field. As a result, the electric quasi-BIC can be effectively excited by an electric dipole. Figure 10(a) shows the mean value of the out-of-plane ED component (p_z) as a function of the lattice period (d) and wavelength of the dipole radiation (λ). The maximum of the mean value of p_z corresponds to the electric dipole quasi-BIC excitation. We can see that the wavelength of the quasi-BIC resonance can be tuned in a broad spectral range by varying the lattice period. Moreover, for a given wavelength, a lattice period corresponding to the excitation of a quasi-BIC is perfectly predicted by Eq. (C1) in Appendix C. In particular, the lattice with $d = 423$ nm supports an electric dipole BIC at a wavelength of $\lambda = 700$ nm. Moreover, this BIC resonance is well pronounced for finite-size $N \times N$ arrays, as shown in Fig. 10(b). One can see that the wavelength of the quasi-BIC resonance reaches the value of 700 nm for $N \gtrsim 17$, which is very close to the value of the resonant wavelength for the corresponding BIC in the infinite array.

V. CONCLUSION

We investigated the collective resonant effects for finite-size 2D arrays of spherical silicon nanoparticles, known as metasurfaces, arising from their dipole coupling. Orienting our theoretical research to experiments, we believed from the very beginning that the particles and metasurfaces were embedded in a homogeneous medium with a refractive index of 1.4. Initially, we outlined the main aspects of an analytical coupled dipole model, which describes the electromagnetic interactions and optical responses in finite and infinite nanoparticle arrays. It is important to mention here that the developed approach of analyzing collective effects in finite and infinite periodic arrays can be extended beyond the dipole approximation [66]. In this case, the emergence of the resonances and array response will be determined by a superposition of multipoles of opposite inversion parities [69].

Subsequently, we demonstrated the utility of the dipole approximation for extracting information about the array period, enabling the observation of resonant phenomena such as the collective Kerker effect and bound state in the continuum for infinite nanoparticle arrays. We note that the conditions of the resonances, namely, Eqs. (10) and (C2), are universal for all geometries of two-dimensional arrays. The main differences will be the change in values of the lattice sums for infinite arrays and the corresponding change of the required lattice period. Additionally, we established the efficient excitation of collective Kerker resonance for finite-size square arrays of nanoparticles by a normally incident plane wave. Notably, the spectral position of this resonance can be finely tuned by adjusting the particle's size or refractive index. Furthermore, we developed a model for the resonance of bound states in the continuum within finite-size arrays of spherical nanoparticles excited by oblique incident plane waves or point dipole sources. Intriguingly, we revealed substantial tunability of the resonance's spectral position across a wide range of wavelengths by altering the array period.

Moreover, for finite-size arrays of $N \times N$ spherical silicon nanoparticles, the development of collective resonances, encompassing lattice Kerker and quasi-BIC resonances, was presented as a function of the N. It was demonstrated that the lattice Kerker resonance emerges in the scattering spectrum of a normally incident plane wave for $N \gtrsim 9$ while its characteristics (amplitude, Q factor, and resonant wavelength) saturate for $N \gtrsim 30$ even in the presence of the in-plane disorder of nanoparticle positions. The quasi-BIC resonance can be excited by a plane wave with a nonzero angle of incidence $\theta_{\rm inc} \neq 0$ because it owns an out-of-plane component of the electric or magnetic fields. In this case, the resonance emerges for $N \gtrsim 11$, and its total Q factor saturates at $N \gtrsim 30$ due to the absorption losses in silicon. Moreover, it was shown that as $\theta_{\rm inc}$ increases, the Q factor of the resonance in a finite-size array decreases as for an infinite array. Considering the excitation of the quasi-BIC with a point dipole source, the

resonance emerges for $N \gtrsim 7$ while its resonant wavelength saturates at $N \gtrsim 17$.

We believe that our results will be essential for designing and optimizing functional photonic structures, whose sizes are always limited in real practical implementations, and motivate experimental demonstration of the considered effects.

ACKNOWLEDGMENTS

N.U. and C.R. acknowledge support through the Deutsche Forschungsgemeinschaft (DFG, German Research Foundation) under Germany's Excellence Strategy via the Excellence Cluster 3D Matter Made to Order (EXC-2082/1, Grant No. 390761711) and from the Carl Zeiss Foundation via CZF-Focus@HEiKA. A.B.E. acknowledges support of the Deutsche Forschungsgemeinschaft (DFG, German Research Foundation) under Germany's Excellence Strategy within the Cluster of Excellence PhoenixD (EXC 2122, Project ID No. 390833453). N.U. also acknowledges support within Erasmus+ program and from region Bourgogne Franche-Comté, France.

APPENDIX A: OPTICAL CROSS SECTIONS AND DIPOLE POLARIZABILITIES OF A SPHERICAL NANOPARTICLE

The extinction and scattering cross sections of a spherical particle illuminated by a linearly polarized, monochromatic plane wave can be expressed analytically via the Mie coefficients [2]

$$\sigma_{0,\mathrm{ext}}(\lambda) = \frac{\lambda^2}{2\pi\varepsilon_S}\sum_{l=1}^{+\infty}(2l+1)\mathrm{Re}[a_l + b_l], \tag{A1}$$

$$\sigma_{0,\mathrm{sca}}(\lambda) = \frac{\lambda^2}{2\pi\varepsilon_S}\sum_{l=1}^{+\infty}(2l+1)(|a_l|^2 + |b_l|^2), \tag{A2}$$

where l is the order of multipole mode such that $l = 1$ is a dipole, $l = 2$ is a quadrupole, etc.

The ED and MD polarizabilities of a spherical nanoparticle are also analytical scalar functions [2]:

$$\alpha_p(\lambda) = i\frac{6\pi\varepsilon_0\varepsilon_S}{k_S^3}a_1, \quad \alpha_m(\lambda) = i\frac{6\pi}{k_S^3}b_1. \tag{A3}$$

Figure 11 shows the inverse polarizabilities used to determine the spectral positions of the collective resonances. One can see that the imaginary parts of the inverse dipole polarizabilities remain almost constant. Indeed, for a dielectric nonabsorbing spherical particle, we can find from the optical theorem that [19]

$$\mathrm{Im}\left[\frac{1}{\alpha_m}\right] = \mathrm{Im}\left[\frac{\varepsilon_0\varepsilon_S}{\alpha_p}\right] = -\frac{k_S^3}{6\pi}. \tag{A4}$$

Figure 11 justifies the use of Eq. (A4) as a good approximation for the imaginary parts of the inverse dipole polarizabilities for a silicon particle since the absorption of c-Si is low.

After comparison of Eqs. (A2) and (A3), one can write the scattering cross section of a single spherical particle in the dipole approximation

$$\sigma_{0,\mathrm{sca}}(\lambda) = \frac{k_S^4}{6\pi\varepsilon_0^2\varepsilon_S^2}|\alpha_p(\lambda)|^2 + \frac{k_S^4}{6\pi}|\alpha_m(\lambda)|^2. \tag{A5}$$

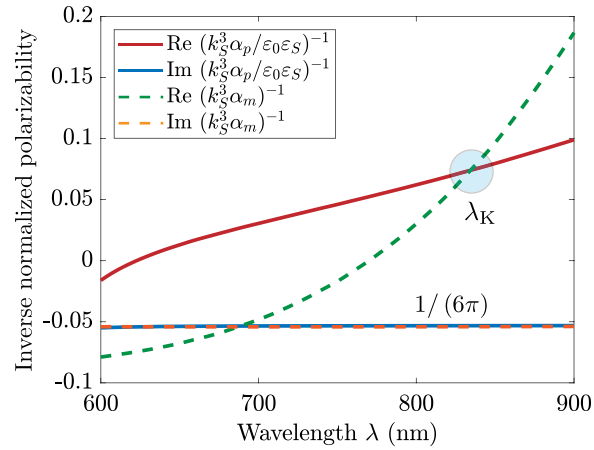

FIG. 11. Inverse normalized (multiplied by factor k_S^3) dipole polarizabilities (A3) for the considered spherical particle. Their imaginary parts are $\mathrm{Im}[(k_S^3\alpha)^{-1}] = 1/(6\pi)$, where $\alpha = \alpha_p/(\varepsilon_0\varepsilon_S)$ or $\alpha = \alpha_m$, in the considered spectral range. The blue circle indicates wavelength $\lambda_K = 834$ nm when the first Kerker condition $\alpha_p/(\varepsilon_0\varepsilon_S) = \alpha_m$ is satisfied; see Sec. III. The values of the wavelength λ are indicated for vacuum.

APPENDIX B: OPTICAL RESPONSE OF A NANOPARTICLE IN INFINITE PERIODIC 2D ARRAYS

In this section, we present the analytical description of the optical response of a nanoparticle in the *infinite* square array (lattice).

In-plane translational symmetry of the infinite lattice implies the Bloch theorem for the particles' dipole moments: $\mathbf{p}_j = \mathbf{p}_0 e^{i\mathbf{k}_\parallel\cdot\mathbf{r}_j}$, $\mathbf{m}_j = \mathbf{m}_0 e^{i\mathbf{k}_\parallel\cdot\mathbf{r}_j}$, where $\mathbf{p}_0$ and $\mathbf{m}_0$ are dipole moments of the particle placed at the coordinate system origin $\mathbf{r}_0 = 0$ and $\mathbf{k}_\parallel = (k_x, k_y, 0)$ is the in-plane wave vector. Let us further consider $\mathbf{k}_\parallel = 0$, which implies that all nanoparticle dipole moments are in phase, corresponding to Γ point of the Brillouin zone. A square periodic lattice of spherical nanoparticles does not support ED-MD coupling under a normal incident plane wave [17,66]. In this case, Eqs. (2) become [2,80]

$$\mathbf{p}_0 = \varepsilon_0\varepsilon_S\underbrace{\left[\frac{\varepsilon_0\varepsilon_S}{\alpha_p}\hat{I} - \hat{S}\right]^{-1}}_{\hat{\alpha}_p^{(\mathrm{eff})}}\mathbf{E}_{\mathrm{inc}}(\mathbf{r}),$$

$$\mathbf{m}_0 = \underbrace{\left[\frac{1}{\alpha_m}\hat{I} - \hat{S}\right]^{-1}}_{\hat{\alpha}_m^{(\mathrm{eff})}}\mathbf{H}_{\mathrm{inc}}(\mathbf{r}), \tag{B1}$$

where $\hat{\alpha}_p^{(\mathrm{eff})}$ and $\hat{\alpha}_m^{(\mathrm{eff})}$ are the ED and MD *effective* polarizabilities of a nanoparticle in the infinite lattice, and $\hat{I}$ is the 3×3 identity matrix. The *lattice sum* tensor $\hat{S}$ considers the electromagnetic ED-ED or MD-MD coupling between particles being a diagonal matrix and for a periodic lattice with a square cell it has the following diagonal form [2]

$$\hat{S} = \begin{pmatrix} S_\parallel & 0 & 0 \\ 0 & S_\parallel & 0 \\ 0 & 0 & S_\perp \end{pmatrix}. \tag{B2}$$

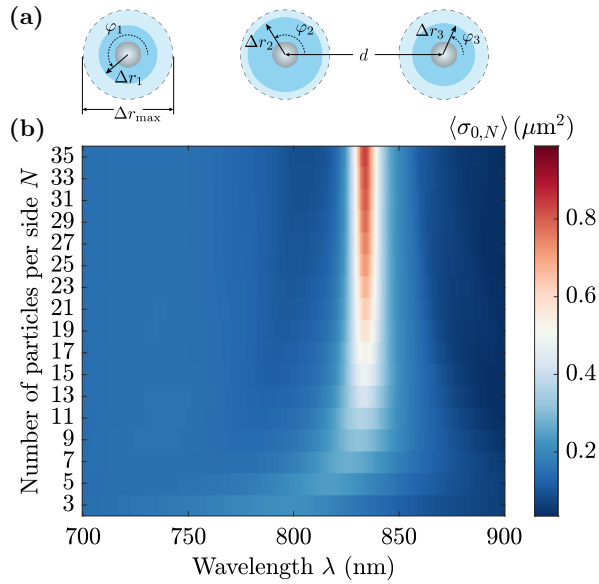

FIG. 12. (a) An array with in-plane disorder of nanoparticle positions. The largest shift of nanoparticle position Δr_j is randomly selected from range $[0, \Delta r_{\max}]$, where the angle φ_j is randomly selected from 0 to 2π. Here, integer j runs from 1 to N_{tot}. (b) Averaged scattering cross-section per particle $\langle\sigma_{0,N}\rangle \equiv \langle\sigma_{\text{sca}}(N)\rangle/N^2$ where $\langle\sigma_{\text{sca}}(N)\rangle$ is the averaged total scattering cross section (6) for the $N \times N$ array with period $d = 577$ nm and $\Delta r_{\max} = 70$ nm. The array is illuminated by an external plane wave, as shown in Fig. 3. The averaging procedure is performed for $N_{\text{iter}} = 10$ configurations of the array. The values of the wavelength λ are indicated for vacuum.

Components of the tensor for in-plane ($\parallel$) and out-of-plane ($\perp$) dipole orientations follow from the expression for the dyadic Green's function:

$$S_\parallel = k_S^2 \sum_{j_x, j_y \neq 0} \frac{e^{ik_S r_j}}{4\pi r_j} \times \left[\left(1 + \frac{i}{k_S r_j} - \frac{1}{k_S^2 r_j^2}\right) + \left(-1 - \frac{i3}{k_S r_j} + \frac{3}{k_S^2 r_j^2}\right)\frac{d^2 j_x^2}{r_j^2}\right],$$

$$S_\perp = k_S^2 \sum_{j_x, j_y \neq 0} \frac{e^{ik_S r_j}}{4\pi r_j}\left(1 + \frac{i}{k_S r_j} - \frac{1}{k_S^2 r_j^2}\right), \tag{B3}$$

where $r_j = d\sqrt{j_x^2 + j_y^2}$. The summation indices j_x and j_y run over all integers excluding zero. These dipole sums depend on the lattice period d, and the wavelength λ/n_S in the surrounding medium $\hat{S} = \hat{S}(d, \lambda/n_S)$ but they are independent of particle characteristics and properties. The latter are incorporated into the single-particle polarizabilities α_p and α_m.

For subdiffraction square lattices ($d < \lambda/n_S$), imaginary parts of these lattice sums can be calculated analytically [41,81]:

$$\text{Im}[S_\parallel] = \frac{k_S}{2d^2} - \frac{k_S^3}{6\pi}, \quad \text{Im}[S_\perp] = -\frac{k_S^3}{6\pi}. \tag{B4}$$

The nanoparticle coupling in the lattice affects only the amplitudes and phases of their dipole moments ($\mathbf{p}_0$ and $\mathbf{m}_0$) but not their radiation patterns of single particles. When nanoparticles are organized into a periodic structure, their radiation properties resemble those of an individual particle. However, the radiation from the lattice occurs only in the direction of open diffraction channels [76]. Indeed, for an infinite array, the summation over particle coordinates $\mathbf{r}_j$ for the radiation pattern (4) can be converted to the sum over reciprocal lattice vectors $\mathbf{q}_m$ determining open diffraction channels: $\sum_{j=0}^{+\infty} e^{-ik_S(\mathbf{n}\cdot\mathbf{r}_j)} = (\frac{2\pi}{d})^2 \sum_m \delta(k_S\mathbf{n}_\parallel - \mathbf{q}_m)$, where $\delta(\dots)$ is the Dirac delta function. Here, $\mathbf{n}_\parallel$ is the projection of $\mathbf{n}$ on the xy-plane. For subwavelength lattice periods $d < \lambda/n_s$, only the zeroth diffraction channel $\mathbf{q}_m = 0$ is open since, for $m \neq 0$, the waves with $|\mathbf{q}_m| > 2\pi\lambda/n_S$ are evanescent in the surrounding medium. Hence, we immediately obtain Eq. (8) of the main text.

APPENDIX C: ANALYTICAL CONDITION OF BICS FOR PERIODIC METASURFACES IN THE DIPOLE APPROXIMATION

The BIC in a dipole lattice can be defined as a nontrivial solution of Eq. (B1) in the absence of external fields, corresponding to a pole of the effective polarizability or, more

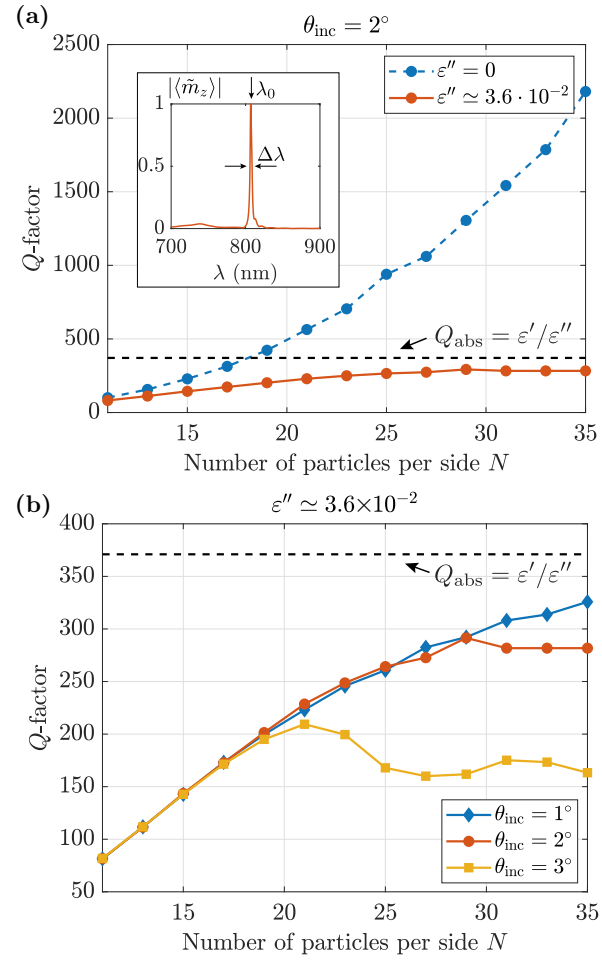

FIG. 13. Development of the *total* quality factor of the magnetic dipole quasi-BIC in finite-size arrays as a function of N for (a) different values of absorption losses in particles, and (b) different angles of incidence. The inset shows the spectrum of the normalized (by a maximal value for certain N) mean z component of MD moments for $N = 35$ at $\theta_{\text{inc}} = 2°$ and with material losses.

general, S matrix of the system [82]. The condition is the following [19,41]:

$$1 - \alpha S_{\perp} = 0, \tag{C1}$$

where $\alpha = \frac{\alpha_p}{\varepsilon_0 \varepsilon_S}$ for electric and $\alpha = \alpha_m$ for magnetic dipole BICs, $S_{\perp}$ is given by Eq. (B3). Equations (A4) and (B4) on the imaginary parts imply that Eq. (C1) can be simplified to

$$\mathrm{Re}\left[\frac{1}{\alpha}\right] = \mathrm{Re}[S_{\perp}] \tag{C2}$$

for subdiffraction lattices.

APPENDIX D: INFLUENCE OF THE DISORDER ON THE COLLECTIVE KERKER RESONANCE

In this Appendix, we investigate the influence of the in-plane disorder of nanoparticle positions on the collective Kerker resonance described in Sec. III of the main text. To do this, we draw around the particle j a circle with an arbitrary radius $\Delta r_j \in [0, \Delta r_{\max}]$ and a center at the point $\mathbf{r}_j = (x_j, y_j)$ as shown in Fig. 12(a). Further, the angle $\varphi_j \in [0, 2\pi)$ is randomly selected. Thus, a new position for the particle j is given by the radius vector $(x_j + \Delta r_j \cos\varphi_j, y_j + \Delta r_j \sin\varphi_j)$, in Fig. 12(a) the solid black arrows point new positions of the nanoparticles. For each configuration of the array with disorder, one can calculate the scattering cross section per particle $\sigma_{0,N}$ as well as in Sec. III. Repeating this procedure N_{iter} times, one can obtain the averaged $\sigma_{0,N}$ shown in Fig. 12(b) for $\Delta r_{\max} = 70$ nm and $N_{\mathrm{iter}} = 10$. The disorder affects only the magnitude of the cross section, but not the qualitative behavior.

APPENDIX E: QUALITY FACTOR OF THE QUASI-BIC IN FINITE-SIZE ARRAYS

To calculate the quality factor of the quasi-BIC (Q factor) as a function of the particle number N per side, investigated in Sec. IV, we consider the (N, λ) map of the mean out-of-plane magnetic dipole component $|\langle m_z \rangle|$ such as shown in Fig. 8 for $\theta_{\mathrm{inc}} = 2^{\circ}$. For each N, we calculate the normalized function of λ, $|\langle \tilde{m}_z \rangle| = |\langle m_z \rangle| / \max_{\lambda} |\langle m_z \rangle|$, which takes values from 0 to 1; see inset in Fig. 13(a). Further, we compute the Q factor as $\lambda_0/\Delta\lambda$ where λ_0 is the wavelength of $|\langle \tilde{m}_z \rangle|$ peak and $\Delta\lambda$ is the peak's full width at half-maximum. The red solid curve in Fig. 13(a) shows the resulting function $Q(N)$ along with a similar function (blue dashed curve) but for arrays without absorption losses. Figure 13(b) also shows the functions $Q(N)$ for arrays with absorption but at different angles of incidences of external plane waves. Moreover, Fig. 13 also shows (black dashed line) the estimated limitation for the Q factor of the quasi-BIC, i.e., $Q(N) \leqslant Q_{\mathrm{abs}}$ for any N, being roughly $Q_{\mathrm{abs}} = \varepsilon'/\varepsilon''$ [55]. The values of the material parameters $\varepsilon' \equiv \mathrm{Re}(\varepsilon)$ and $\varepsilon'' \equiv \mathrm{Im}(\varepsilon)$ are taken for crystalline silicon at vacuum wavelength $\lambda = 808$ nm of the BIC resonance in the infinite array, that results in $Q_{\mathrm{abs}} = 370$. The actual value of the maximal Q factor is less than Q_{abs} because, to be more precise, $Q_{\max} = Q_{\mathrm{abs}}/C$ where C is the fraction of electric energy stored inside the particles [56].

[1] K. Koshelev and Y. Kivshar, Dielectric resonant metaphotonics, ACS Photonics **8**, 102 (2021).

[2] A. B. Evlyukhin, C. Reinhardt, A. Seidel, B. S. Luk'yanchuk, and B. N. Chichkov, Optical response features of Si-nanoparticle arrays, Phys. Rev. B **82**, 045404 (2010).

[3] A. García-Etxarri, R. Gómez-Medina, L. S. Froufe-Pérez, C. López, L. Chantada, F. Scheffold, J. Aizpurua, M. Nieto-Vesperinas, and J. J. Sáenz, Strong magnetic response of submicron Silicon particles in the infrared, Opt. Express **19**, 4815 (2011).

[4] A. B. Evlyukhin, S. M. Novikov, U. Zywietz, R. L. Eriksen, C. Reinhardt, S. I. Bozhevolnyi, and B. N. Chichkov, Demonstration of magnetic dipole resonances of dielectric nanospheres in the visible region, Nano Lett. **12**, 3749 (2012).

[5] A. I. Kuznetsov, A. E. Miroshnichenko, Y. H. Fu, J. Zhang, and B. Luk'yanchuk, Magnetic light, Sci. Rep. **2**, 492 (2012).

[6] G. Mie, Beiträge zur Optik trüber Medien, speziell kolloidaler Metallösungen, Ann. Phys. **330**, 377 (1908).

[7] A. I. Kuznetsov, A. E. Miroshnichenko, M. L. Brongersma, Y. S. Kivshar, and B. Luk'yanchuk, Optically resonant dielectric nanostructures, Science **354**, aag2472 (2016).

[8] A. B. Evlyukhin, C. Reinhardt, E. Evlyukhin, and B. N. Chichkov, Multipole analysis of light scattering by arbitrary-shaped nanoparticles on a plane surface, J. Opt. Soc. Am. B **30**, 2589 (2013).

[9] A. B. Evlyukhin, T. Fischer, C. Reinhardt, and B. N. Chichkov, Optical theorem and multipole scattering of light by arbitrarily shaped nanoparticles, Phys. Rev. B **94**, 205434 (2016).

[10] M. Kerker, D.-S. Wang, and C. L. Giles, Electromagnetic scattering by magnetic spheres, J. Opt. Soc. Am. **73**, 765 (1983).

[11] S. Person, M. Jain, Z. Lapin, J. J. Sáenz, G. Wicks, and L. Novotny, Demonstration of zero optical backscattering from single nanoparticles, Nano Lett. **13**, 1806 (2013).

[12] P. R. Wiecha, A. Cuche, A. Arbouet, C. Girard, G. Colas des Francs, A. Lecestre, G. Larrieu, F. Fournel, V. Larrey, T. Baron, and V. Paillard, Strongly directional scattering from dielectric nanowires, ACS Photonics **4**, 2036 (2017).

[13] Y. H. Fu, A. I. Kuznetsov, A. E. Miroshnichenko, Y. F. Yu, and B. Luk'yanchuk, Directional visible light scattering by silicon nanoparticles, Nat. Commun. **4**, 1527 (2013).

[14] A. B. Evlyukhin, C. Reinhardt, and B. N. Chichkov, Multipole light scattering by nonspherical nanoparticles in the discrete dipole approximation, Phys. Rev. B **84**, 235429 (2011).

[15] I. Staude, A. E. Miroshnichenko, M. Decker, N. T. Fofang, S. Liu, E. Gonzales, J. Dominguez, T. S. Luk, D. N. Neshev, I. Brener, and Y. Kivshar, Tailoring directional scattering through magnetic and electric resonances in subwavelength silicon nanodisks, ACS Nano **7**, 7824 (2013).

[16] B. Lamprecht, G. Schider, R. T. Lechner, H. Ditlbacher, J. R. Krenn, A. Leitner, and F. R. Aussenegg, Metal nanoparticle

gratings: Influence of dipolar particle interaction on the plasmon resonance, Phys. Rev. Lett. **84**, 4721 (2000).

[17] A. Rahimzadegan, T. D. Karamanos, R. Alaee, A. G. Lamprianidis, D. Beutel, R. W. Boyd, and C. Rockstuhl, A comprehensive multipolar theory for periodic metasurfaces, Adv. Opt. Mater. **10**, 2102059 (2022).

[18] B. Auguié and W. L. Barnes, Collective resonances in gold nanoparticle arrays, Phys. Rev. Lett. **101**, 143902 (2008).

[19] A. B. Evlyukhin, M. A. Poleva, A. V. Prokhorov, K. V. Baryshnikova, A. E. Miroshnichenko, and B. N. Chichkov, Polarization switching between electric and magnetic quasi-trapped modes in bianisotropic all-dielectric metasurfaces, Laser Photon. Rev. **15**, 2100206 (2021).

[20] P. D. Terekhov, V. E. Babicheva, K. V. Baryshnikova, A. S. Shalin, A. Karabchevsky, and A. B. Evlyukhin, Multipole analysis of dielectric metasurfaces composed of nonspherical nanoparticles and lattice invisibility effect, Phys. Rev. B **99**, 045424 (2019).

[21] V. E. Babicheva and A. B. Evlyukhin, Metasurfaces with electric quadrupole and magnetic dipole resonant coupling, ACS Photonics **5**, 2022 (2018).

[22] V. Karimi and V. E. Babicheva, Dipole-lattice nanoparticle resonances in finite arrays, Opt. Express **31**, 16857 (2023).

[23] T. Liu, R. Xu, P. Yu, Z. Wang, and J. Takahara, Multipole and multimode engineering in Mie resonance-based metastructures, Nanophotonics **9**, 1115 (2020).

[24] S. D. Swiecicki and J. E. Sipe, Surface-lattice resonances in two-dimensional arrays of spheres: Multipolar interactions and a mode analysis, Phys. Rev. B **95**, 195406 (2017).

[25] V. G. Kravets, A. V. Kabashin, W. L. Barnes, and A. N. Grigorenko, Plasmonic surface lattice resonances: A review of properties and applications, Chem. Rev. **118**, 5912 (2018).

[26] T. Jensen, L. Kelly, A. Lazarides, and G. C. Schatz, Electrodynamics of noble metal nanoparticles and nanoparticle clusters, J. Cluster Sci. **10**, 295 (1999).

[27] S. Zou, N. Janel, and G. C. Schatz, Silver nanoparticle array structures that produce remarkably narrow plasmon lineshapes, J. Chem. Phys. **120**, 10871 (2004).

[28] J. Sung, E. M. Hicks, R. P. Van Duyne, and K. G. Spears, Nanoparticle spectroscopy: Plasmon coupling in finite-sized two-dimensional arrays of cylindrical silver nanoparticles, J. Phys. Chem. C **112**, 4091 (2008).

[29] S. R. K. Rodriguez, G. Lozano, M. A. Verschuuren, R. Gomes, K. Lambert, B. De Geyter, A. Hassinen, D. Van Thourhout, Z. Hens, and J. Gómez Rivas, Quantum rod emission coupled to plasmonic lattice resonances: A collective directional source of polarized light, Appl. Phys. Lett. **100**, 111103 (2012).

[30] J.-P. Martikainen, A. J. Moilanen, and P. Törmä, Coupled dipole approximation across the Γ-point in a finite-sized nanoparticle array, Philos. Trans. R. Soc. A. **375**, 20160316 (2017).

[31] L. Zundel and A. Manjavacas, Finite-size effects on periodic arrays of nanostructures, J. Phys. Photonics **1**, 015004 (2018).

[32] D. Wang, M. R. Bourgeois, J. Guan, A. K. Fumani, G. C. Schatz, and T. W. Odom, Lasing from finite plasmonic nanoparticle lattices, ACS Photonics **7**, 630 (2020).

[33] L. Zundel, J. R. Deop-Ruano, R. Martinez-Herrero, and A. Manjavacas, Lattice resonances excited by finite-width light beams, ACS Omega **7**, 31431 (2022).

[34] A. D. Utyushev, V. I. Zakomirnyi, and I. L. Rasskazov, Collective lattice resonances: Plasmonics and beyond, Rev. Phys. **6**, 100051 (2021).

[35] A. S. Kostyukov, I. L. Rasskazov, V. S. Gerasimov, S. P. Polyutov, S. V. Karpov, and A. E. Ershov, Multipolar lattice resonances in plasmonic finite-size metasurfaces, Photonics **8**, 109 (2021).

[36] I. Allayarov, A. B. Evlyukhin, and A. C. Lesina, Multiresonant all-dielectric metasurfaces based on high-order multipole coupling in the visible, Opt. Express **32**, 5641 (2024).

[37] V. E. Babicheva and A. B. Evlyukhin, Resonant lattice Kerker effect in metasurfaces with electric and magnetic optical responses, Laser Photonics Rev. **11**, 1700132 (2017).

[38] A. Sobhani, M. W. Knight, Y. Wang, B. Zheng, N. S. King, L. V. Brown, Z. Fang, P. Nordlander, and N. J. Halas, Narrowband photodetection in the near-infrared with a plasmon-induced hot electron device, Nat. Commun. **4**, 1643 (2013).

[39] P. Offermans, M. C. Schaafsma, S. R. K. Rodriguez, Y. Zhang, M. Crego-Calama, S. H. Brongersma, and J. Gómez Rivas, Universal scaling of the figure of merit of plasmonic sensors, ACS Nano **5**, 5151 (2011).

[40] C. W. Hsu, B. Zhen, A. D. Stone, J. D. Joannopoulos, and M. Soljačić, Bound states in the continuum, Nat. Rev. Mater. **1**, 16048 (2016).

[41] A. B. Evlyukhin, V. R. Tuz, V. S. Volkov, and B. N. Chichkov, Bianisotropy for light trapping in all-dielectric metasurfaces, Phys. Rev. B **101**, 205415 (2020).

[42] K. L. Koshelev, Z. F. Sadrieva, A. A. Shcherbakov, Y. S. Kivshar, and A. A. Bogdanov, Bound states in the continuum in photonic structures, Phys. Usp. **66**, 494 (2023).

[43] S. Gladyshev, T. D. Karamanos, L. Kuhn, D. Beutel, T. Weiss, C. Rockstuhl, and A. Bogdanov, Inverse design of all-dielectric metasurfaces with accidental bound states in the continuum, Nanophotonics **12**, 3767 (2023).

[44] E. N. Bulgakov and D. N. Maksimov, Light enhancement by quasi-bound states in the continuum in dielectric arrays, Opt. Express **25**, 14134 (2017).

[45] K. Koshelev, Y. Tang, K. Li, D.-Y. Choi, G. Li, and Y. Kivshar, Nonlinear metasurfaces governed by bound states in the continuum, ACS Photonics **6**, 1639 (2019).

[46] A. Kodigala, T. Lepetit, Q. Gu, B. Bahari, Y. Fainman, and B. Kanté, Lasing action from photonic bound states in continuum, Nature (London) **541**, 196 (2017).

[47] A. Tittl, A. Leitis, M. Liu, F. Yesilkoy, D.-Y. Choi, D. N. Neshev, Y. S. Kivshar, and H. Altug, Imaging-based molecular barcoding with pixelated dielectric metasurfaces, Science **360**, 1105 (2018).

[48] Y. Jahani, E. R. Arvelo, F. Yesilkoy, K. Koshelev, C. Cianciaruso, M. De Palma, Y. Kivshar, and H. Altug, Imaging-based spectrometer-less optofluidic biosensors based on dielectric metasurfaces for detecting extracellular vesicles, Nat. Commun. **12**, 3246 (2021).

[49] A. Leitis, A. Tittl, M. Liu, B. H. Lee, M. B. Gu, Y. S. Kivshar, and H. Altug, Angle-multiplexed all-dielectric metasurfaces for broadband molecular fingerprint retrieval, Sci. Adv. **5**, eaaw2871 (2019).

[50] S. R. K. Rodriguez, M. C. Schaafsma, A. Berrier, and J. Gómez Rivas, Collective resonances in plasmonic crystals: Size matters, Phys. B: Condens. Matter **407**, 4081 (2012).

[51] A. D. Utyushev, V. I. Zakomirnyi, A. E. Ershov, V. S. Gerasimov, S. V. Karpov, and I. L. Rasskazov, Collective lattice resonances in all-dielectric nanostructures under oblique incidence, Photonics **7**, 24 (2020).

[52] D. M. Natarov, V. O. Byelobrov, R. Sauleau, T. M. Benson, and A. I. Nosich, Periodicity-induced effects in the scattering and absorption of light by infinite and finite gratings of circular silver nanowires, Opt. Express **19**, 22176 (2011).

[53] V. I. Zakomirnyi, A. E. Ershov, V. S. Gerasimov, S. V. Karpov, H. Ågren, and I. L. Rasskazov, Collective lattice resonances in arrays of dielectric nanoparticles: a matter of size, Opt. Lett. **44**, 5743 (2019).

[54] V. A. Fedotov, N. Papasimakis, E. Plum, A. Bitzer, M. Walther, P. Kuo, D. P. Tsai, and N. I. Zheludev, Spectral collapse in ensembles of metamolecules, Phys. Rev. Lett. **104**, 223901 (2010).

[55] Z. F. Sadrieva, M. A. Belyakov, M. A. Balezin, P. V. Kapitanova, E. A. Nenasheva, A. F. Sadreev, and A. A. Bogdanov, Experimental observation of a symmetry-protected bound state in the continuum in a chain of dielectric disks, Phys. Rev. A **99**, 053804 (2019).

[56] M. Mikhailovskii, M. Poleva, N. Solodovchenko, M. Sidorenko, Z. Sadrieva, M. Petrov, A. Bogdanov, and R. Savelev, Engineering of high-Q states via collective mode coupling in chains of Mie resonators, arXiv:2312.07007.

[57] C. F. Bohren and D. R. Huffman, *Absorption and Scattering of Light by Small Particles* (Wiley, New York, 1998).

[58] V. E. Babicheva and A. B. Evlyukhin, Multipole lattice effects in high refractive index metasurfaces, J. Appl. Phys. **129**, 040902 (2021).

[59] D. G. Baranov, D. A. Zuev, S. I. Lepeshov, O. V. Kotov, A. E. Krasnok, A. B. Evlyukhin, and B. N. Chichkov, All-dielectric nanophotonics: the quest for better materials and fabrication techniques, Optica **4**, 814 (2017).

[60] U. Zywietz, A. B. Evlyukhin, C. Reinhardt, and B. N. Chichkov, Laser printing of silicon nanoparticles with resonant optical electric and magnetic responses, Nat. Commun. **5**, 3402 (2014).

[61] C. Schinke, P. Christian Peest, J. Schmidt, R. Brendel, K. Bothe, M. R. Vogt, I. Kröger, S. Winter, A. Schirmacher, S. Lim, H. T. Nguyen, and D. MacDonald, Uncertainty analysis for the coefficient of band-to-band absorption of crystalline silicon, AIP Adv. **5**, 067168 (2015).

[62] M. Matiushechkina, A. B. Evlyukhin, V. A. Zenin, M. Heurs, and B. N. Chichkov, High-efficiency silicon metasurface mirror on a sapphire substrate, Opt. Mater. **138**, 113618 (2023).

[63] O. Merchiers, F. Moreno, F. Gonzalez, and J. M. Saiz, Light scattering by an ensemble of interacting dipolar particles with both electric and magnetic polarizabilities, Phys. Rev. A **76**, 043834 (2007).

[64] N. A. Ustimenko, D. F. Kornovan, K. V. Baryshnikova, A. B. Evlyukhin, and M. I. Petrov, Multipole Born series approach to light scattering by Mie-resonant nanoparticle structures, J. Opt. **24**, 035603 (2022).

[65] L. Novotny and B. Hecht, *Principles of Nano-Optics* (Cambridge University Press, Cambridge, 2006).

[66] V. E. Babicheva and A. B. Evlyukhin, Analytical model of resonant electromagnetic dipole-quadrupole coupling in nanoparticle arrays, Phys. Rev. B **99**, 195444 (2019).

[67] R. A. de la Osa, P. Albella, J. M. Saiz, F. Gonzalez, and F. Moreno, Extended discrete dipole approximation and its application to bianisotropic media, Opt. Express **18**, 23865 (2010).

[68] P. R. Wiecha, A. Cuche, H. Kallel, G. C. des Francs, A. Lecestre, G. Larrieu, V. Larrey, F. Fournel, T. Baron, A. Arbouet, and V. Paillard, Fano-resonances in high index dielectric nanowires for directional scattering, in *Fano Resonances in Optics and Microwaves* (Springer, Cham, 2018), pp. 283–309.

[69] H. Ma, A. B. Evlyukhin, A. E. Miroshnichenko, F. Zhu, S. Duan, J. Wu, C. Zhang, J. Chen, B. Jin, W. J. Padilla, and K. Fan, Extremely thin perfect absorber by generalized multipole bianisotropic effect, Adv. Opt. Mater. **12**, 2301968 (2024).

[70] D. Beutel, I. Fernandez-Corbaton, and C. Rockstuhl, Unified lattice sums accommodating multiple sublattices for solutions of the Helmholtz equation in two and three dimensions, Phys. Rev. A **107**, 013508 (2023).

[71] D. Beutel, I. Fernandez-Corbaton, and C. Rockstuhl, *treams* – A T-matrix-based scattering code for nanophotonics, Comput. Phys. Commun. **297**, 109076 (2024).

[72] R. W. Wood, XLII. On a remarkable case of uneven distribution of light in a diffraction grating spectrum, London, Edinburgh, Dublin Philos. Mag., J. Sci. **4**, 396 (1902).

[73] L. Rayleigh, III. Note on the remarkable case of diffraction spectra described by Prof. Wood, London, Edinburgh, Dublin Philos. Mag., J. Sci. **14**, 60 (1907).

[74] R. J. Potton, Reciprocity in optics, Rep. Prog. Phys. **67**, 717 (2004).

[75] Z. Sadrieva, K. Frizyuk, M. Petrov, Y. Kivshar, and A. Bogdanov, Multipolar origin of bound states in the continuum, Phys. Rev. B **100**, 115303 (2019).

[76] S. Gladyshev, A. Shalev, K. Frizyuk, K. Ladutenko, and A. Bogdanov, Bound states in the continuum in multipolar lattices, Phys. Rev. B **105**, L241301 (2022).

[77] K. Koshelev, S. Lepeshov, M. Liu, A. Bogdanov, and Y. Kivshar, Asymmetric metasurfaces with high-Q resonances governed by bound states in the continuum, Phys. Rev. Lett. **121**, 193903 (2018).

[78] R. Kolkowski and A. Shevchenko, Enabling infinite Q factors in absorbing optical systems, Nanophotonics **12**, 3443 (2023).

[79] C. W. Hsu, B. Zhen, J. Lee, S.-L. Chua, S. G. Johnson, J. D. Joannopoulos, and M. Soljačić, Observation of trapped light within the radiation continuum, Nature (London) **499**, 188 (2013).

[80] X. M. Bendaña and F. J. G. de Abajo, Confined collective excitations of self-standing and supported planar periodic particle arrays, Opt. Express **17**, 18826 (2009).

[81] F. J. Garcia De Abajo, *Colloquium*: Light scattering by particle and hole arrays, Rev. Mod. Phys. **79**, 1267 (2007).

[82] S. G. Tikhodeev, A. L. Yablonskii, E. A. Muljarov, N. A. Gippius, and T. Ishihara, Quasiguided modes and optical properties of photonic crystal slabs, Phys. Rev. B **66**, 045102 (2002).